Journal of the Korean Nuclear Society
Volume 25, Number 1, March 1993

Generation of Gamma-Ray Streaming Kernels Through Cylindrical Ducts Via Monte Carlo Method

Dong Su Kim
Korea Power Engineering Company, Inc.

Nam Zin Cho
Korea Advanced Institute of Science and Technology

(Received July 21, 1992)

몬테칼로 방법을 이용한 원통형 관통부의 감마선 스트리밍 커널의 산출

김동수
한국전력기술주식회사

조남진
한국과학기술원

(1992. 7. 21 접수)

Abstract

Radiation streaming through penetrations has been of great concern in radiation shielding design and analysis. This study developed a Monte Carlo method and constructed a data library of results calculated by the Monte Carlo method for radiation streaming through a straight cylindrical duct in concrete walls of a broad, mono-directional, mono-energetic gamma-ray beam of unit intensity. It was demonstrated that average dose rate due to an isotropic point source at arbitrary positions can be well approximated using the library with acceptable error. Thus, the library can be used for efficient analysis of radiation streaming due to arbitrary distributions of gamma-ray sources.

요 약

원자력발전소에는 방사선 차폐체를 통한 수 많은 관통부들이 존재하며, 이를 통한 방사선 스트리밍의 해석은 발전소 작업자들의 방호를 위한 차폐 설계에 있어 중요한 고려사항 중 하나이다. 본 연구에서는 관통부 중 주종을 이루는 콘크리트 벽체 내 원통형 직관통부로 단방향, 단일 에너지의 감마선 면선원에 의한 방사선 스트리밍 해석을 위하여 몬테칼로방법에 따른 전산 프로그램을 개발하였으며, 이를 사용하여 여러 경우의 감마선원 에너지와 입사각, 관통부의 반경과 길이에 대하여 관통부 출구에서의 평균 선량을 계산하여 그 결과를 라이브러리화 하였다. 또한, 이를 이용하여 등방향 점선원에 대하여 적절히 근사할 수 있음을 보임으로서 임의의 감마선원 분포에 대하여 짧은 전산시간으로 정확한 결과를 구할 수 있는 방법을 제공하였다.

1. Introduction

There are about tens of thousands of penetrations through radiation shielding structures in a commercial nuclear power plant, such as electrical conduits, air ventilation ducts, fluid transfer pipes, pressure relief openings, or personnel entry ways. Since penetrations are unavoidable and in many instances radiation streaming through penetrations is the critical consideration in protection against exposure of personnel, the radiation streaming has been one of the important and difficult problems throughout radiation shielding design and analysis.

Most of the penetrations are straight cylindrical ducts vertical to concrete shielding walls, which are objects of this study. Moreover, the ducts are assumed here to be air-filled and unlined, since it is the worst case. The radiation streaming through such a duct may be analysed by *single scattering method*,[1] *Albedo method*,[2,3] and *Monte Carlo method*.[4-9] But they may be used for order-of-magnitude calculations where sufficient margin is available, except the Monte Calro method which is accurate but requires a lot of computing time.[10]

The more accurate the result of an analysis is to be, the more computing time is required. The purpose of this study is to develop a Monte Carlo method and to construct a data library of results calculated by the Monte Carlo method in order to obtain efficiency and accuracy at the same time due to the use of the library in analyzing the radiation streaming through a straight cylindrical duct in concrete walls.

2. Streaming Kernels

Consider a radiation streaming problem through a straight cylindrical duct in an infinite concrete slab of thickness p with a monoenergetic, isotropic γ-ray point source, $S_{pt}(\rho, \zeta, E)$—called *point source* from now on—which is placed as shown in Figure 2.1. Let us define

$$X_{pt}(\rho, \zeta, E; r_0, p) \equiv \text{average dose rate over the duct crosssectional area at duct outlet due to a unit point source} \quad (2.1)$$

If the X_{pt} values are known, it might be straightforward to calculate the dose rates for arbitrary source distributions whose small part can be considered to be an isotropic point source. This study is to determine the X_{pt} values with accuracy sufficient for shielding analysis. The variables are, however, too many to directly calculate the X_{pt} values by Monte Carlo method.

Consider another γ-ray streaming problem with the same configuration as above, except that the source term is a broad, monodirectional, monoenergetic beam of particles incident upon the wall with an angle ζ, $S_{pl}(\zeta, E)$—called *plane source* from now on—as shown in Figure 2.2. Define

$$X_{pl}(\zeta, E; r_0, p) \equiv \text{average dose rate over the duct crosssectional area at duct outlet due to a unit plane source} \quad (2.2)$$

$$K_{pl}(\zeta, E; r_0, p) \equiv \cos\zeta \, X_{pl}(\zeta, E; r_0, p) \quad (2.3)$$

The unit plane source generates one particle per unit time per unit area of the wall surface. Then K_{pl} becomes the dose rate due to the parallel beam of unit intensity, i.e., one particle per unit time per unit area normal to the beam. K_{pl} will be called *streaming kernel of plane source* or simply *plane streaming kernel*.

In the case of isotropic point source, the radiation intensity is reduced by two reasons as the distance from the source point increases—1) material attenuation, and 2) geometrical attenuation according to the inverse-square-law. Let us suppose X_{pt} can be written as

$$X_{pt}(\rho, \zeta, E; r_0, p) = \frac{K_{pt}(\rho, \zeta, E; r_0, p)}{4\pi\rho^2}, \quad (2.4)$$

then K_{pl} might be considered to be the dose rate when only the material attenuation is considered. K_{pl} will be called *streaming kernel of point source* or simply *point streaming kernel.*

Let us now suppose with some bravery that X_{pl} can be approximated by K_{pl}, since there is only the material attenuation in the case of plane source. It is intuitively recognized that the dose rate X_{pl} asymtotically approaches $\cos\zeta\ X_{pl}/4\pi\rho^2$ as ρ increases, i.e.,

$$\lim_{\rho\to\infty} 4\pi\rho^2 X_{pt}(\rho,\zeta,E;r_0,p) = \cos\zeta\, X_{pl}(\zeta,E;r_0,p). \quad (2.5)$$

Then, in view of Eqs. (2.3) and (2.4)

$$\lim_{\rho\to\infty} K_{pt}(\rho,\zeta,E;r_0,p) = K_{pl}(\zeta,E;r_0,p). \quad (2.6)$$

Thus, If the assumption

$$K_{pt}(\rho,\zeta,E;r_0,p) \approx K_{pl}(\zeta,E;r_0,p) \quad (2.7)$$

is justified (see Section 5), the effort of calculation can be reduced greatly, since the number of variables is reduced from five to four. Once K_{pl} is determined by the Monte Carlo method, X_{pt} can be obtained as

$$X_{pt}(\rho,\zeta,E;r_0,p) \approx \frac{K_{pl}(\zeta,E;r_0,p)}{4\pi\rho^2}, \quad (2.8)$$

and then using this the streaming problem can be analyzed efficiently for an arbitrary distribution of γ-ray isotropic source.

3. Simulation with the Monte Carlo Method

On the basis of the Monte Carlo method, two computer programs were written separately for the plane source and point source, which are named as *DOGPL* and *DOGPT*, respectively. The procedures and algorithms of the two programs are essentially the same with the exception of the ways how to sample the source particles. The procedures are summarized in Table 3.1.

The positions, directional angles, and energies of the particles are treated with continuous variables through their random walks. The macroscopic cross sections of concrete are obtained from the mass attenuation coefficients in reference 10. To estimate the average dose rate over the duct crosssectional area at the duct outlet, either X_{pt} or X_{pl}, a surface crossing estimator[14] is used with the flux-to-dose conversion factors in reference 11. The programs were written in Fortran77 mounted on a SPARK workstation of Sun Mic-

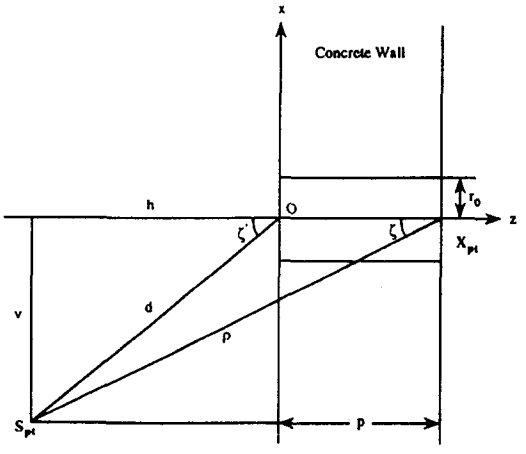

Fig.2.1. Dose Rate due to a Point Source

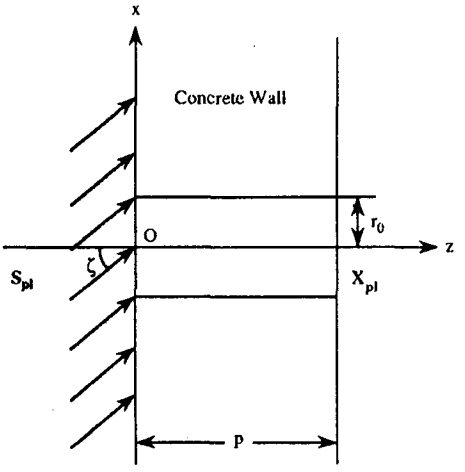

Fig.2.2. Dose Rate due to a Point Source

Table 3.1. Procedures of Monte Carlo Simulation

1. Determine geometric variables.
2. Sample a source particle.
3. Simulate random walks.
   - i) Calculate the distance to the duct boundary.
   - ii) Sample a streaming length to the next collision.
   - iii) Score if the path line intersects the duct cross sectional area at outlet.
   - iv) Determine the next collision point
     If the collision point is out of the system, kill it and go to xi).
   - v) Reduce the particle weight for the implicit photoelectric effect.
   - vi) Weight cutoff and Russian Roulette.
   - vii) Geometric splitting and Russian Roulette.
   - viii) Sample a collision type among Compton scattering and pair-production.
     If Compton scattering, sample a new direction and an energy from the *Klein-Nishina* distribution by the *Kahn's* method.[12,13]
     If pair-production, sample a new direction from isotropic distribution, make its energy 0.511 MeV and double its weight.
   - ix) Energy cutoff (0.01 MeV$\leq E \leq$10 MeV).
   - x) Determine cross section data for the new energy, and go to i).
   - xi) If the particle is killed at iv), vi), vii), and ix), go to viii) when there are particles in the *BANK*, or terminate the random walk otherwise.
4. Test whether or not the variance is reduced within a given criterion. If not, go to 2.
5. Stop the run.

rosystems, Inc. The random number generator used in the programs is one built in the compiler, named as FUNCTION RAND( ) that is a non-linear additive feedback random number generator.

4. Results of Plane Streaming Kernel

The plane streaming kernel $K_{pl}(\zeta, E; r_o, p)$ has been evaluated for 20 source energies(E) from 0.05 to 10MeV, 36 source incident angles(ζ) from 0 to 70 degrees, 5 duct radii(r_o) from 10 to 30cm, and 16 wall thicknesses(p) from 0 to 100cm with the computer program *DOGPL*. The quantity of the data is too large to represent here in full. They are, therefore, plotted in Figures 4.1 thru 4.3 according to the source incident angle for the duct radii of 10, 20, and 30cm. Figures 4.4 and 4.5 shows the plot of the plane streaming kernel with wall thickness and source energy as abscissa, respectively, for the duct radius of 10 cm.

Some irregularities are shown on the curves of the figures, that are considered to result from the statistical fluctuation, although the relative error R, defined as below, was limited within 5%.

$$R \equiv \frac{s_{\bar{x}}}{\sqrt{N}\hat{X}} = \frac{1}{\hat{X}}\sqrt{\frac{\hat{X^2} - \hat{X}^2}{N-1}} \tag{4.1}$$

where N is the number of source particles sampled, and $\hat{X}$ and s_x^2 are sample mean and variance. It was experienced during the calculations that statistical error generally increases as

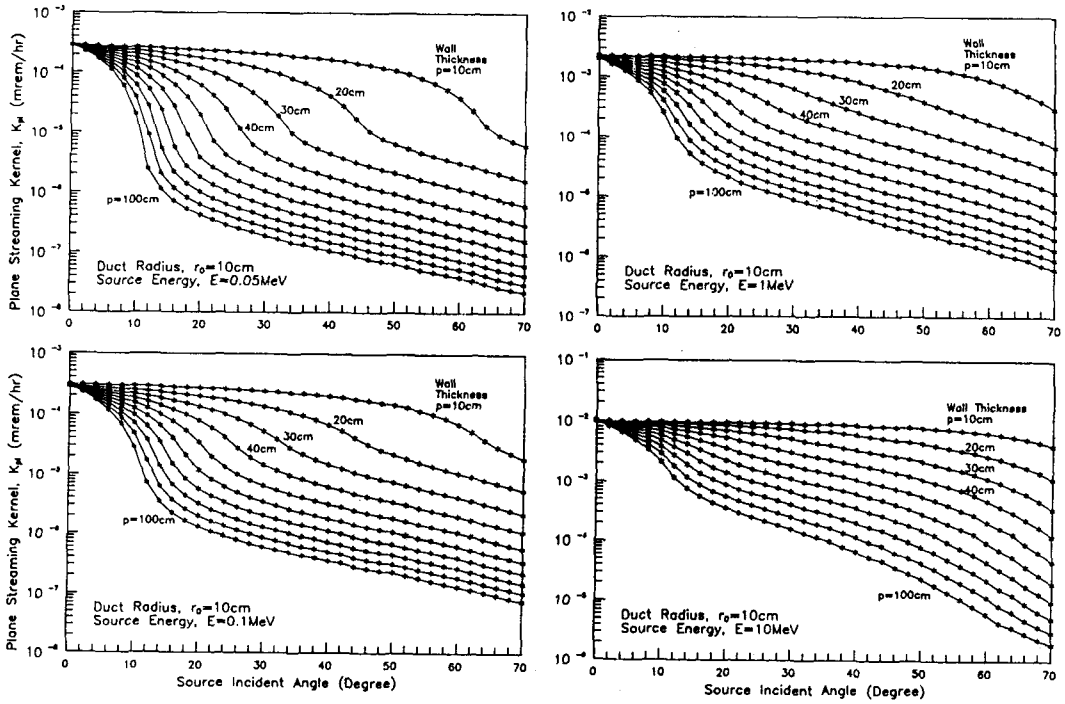

Fig.4.1. Plane Streaming Kernel vs. Incident Angle for Duct of Radius r_o=10 cm

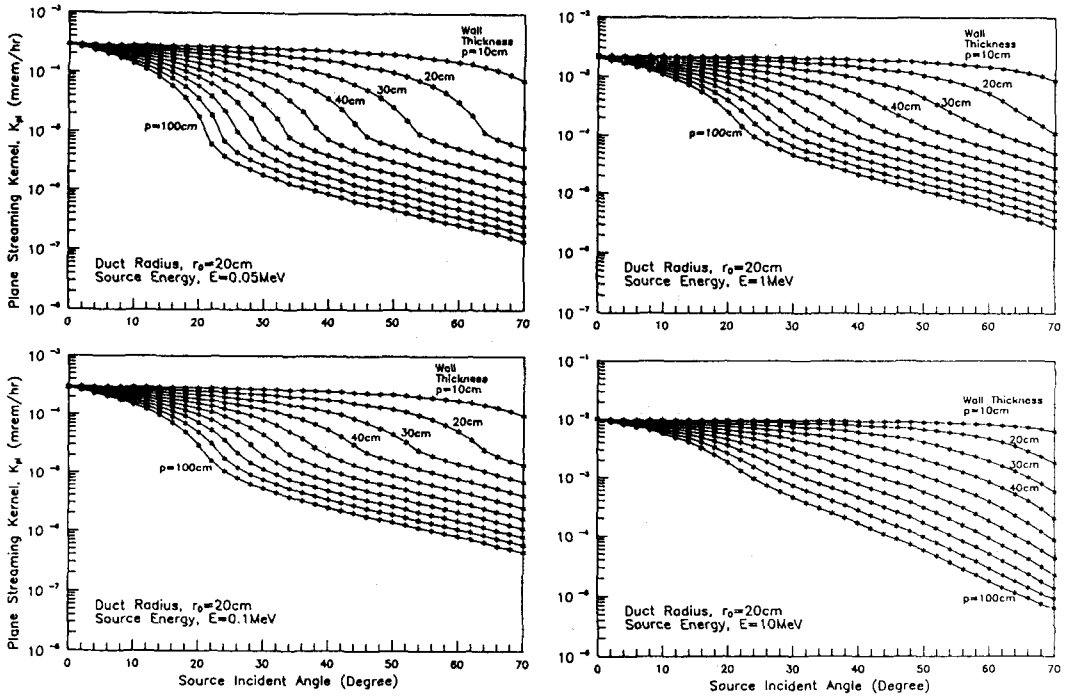

Fig.4.2. Plane Streaming Kernel vs. Incident Angle for Duct of Radius r_o=20 cm

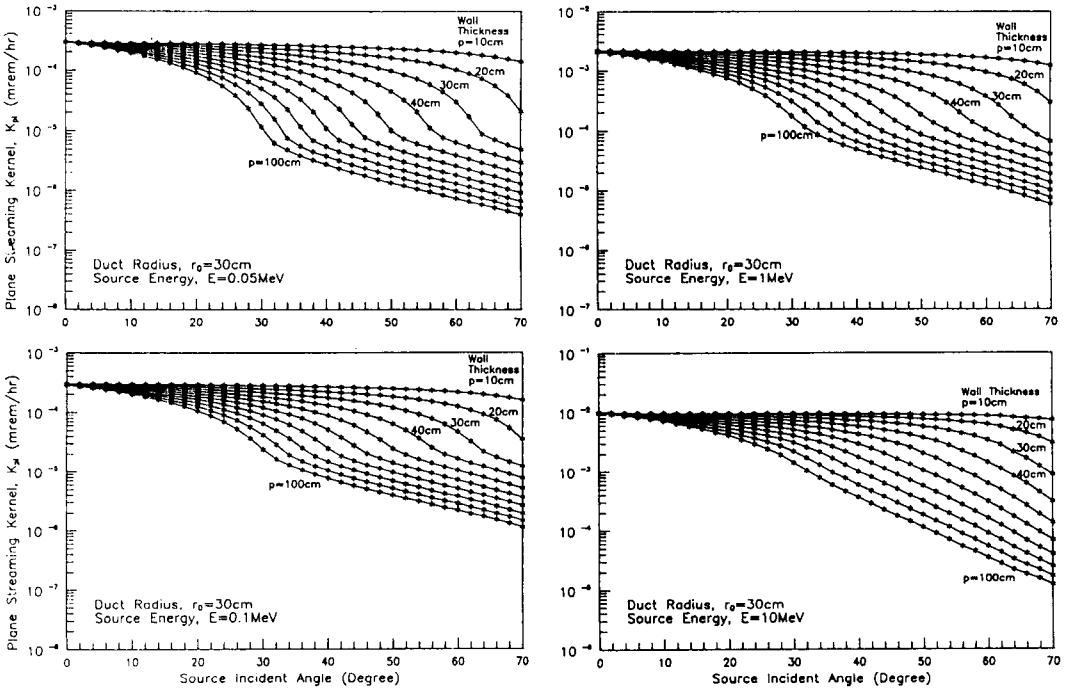

Fig.4.3. Plane Streaming Kernel vs. Incident Angle for Duct of Radius r_o = 30 cm

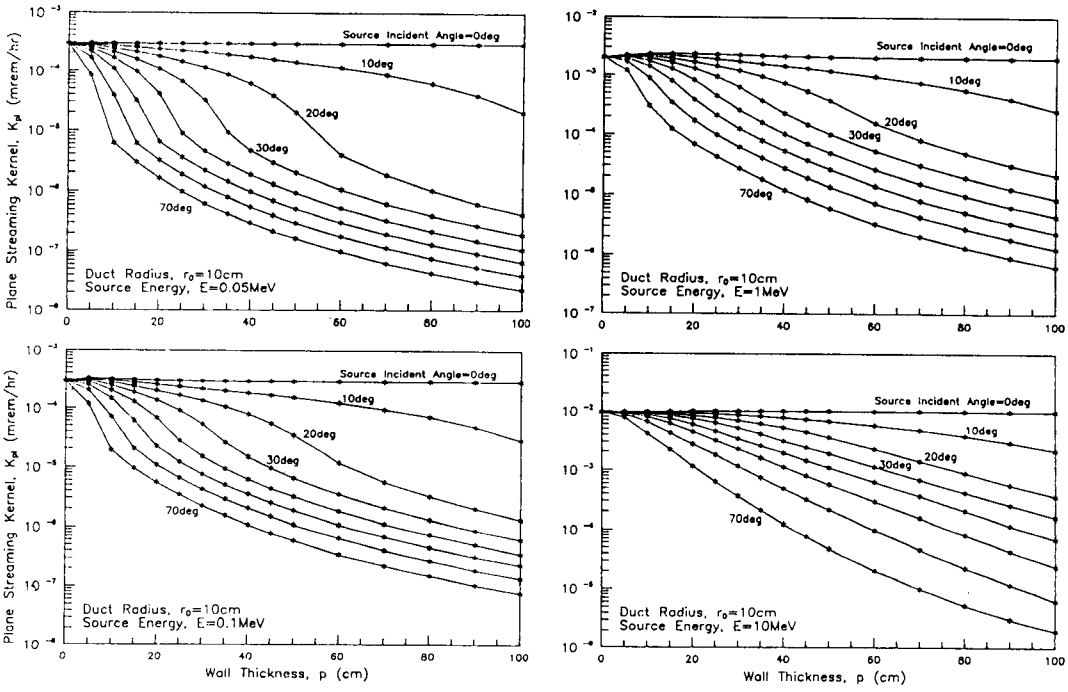

Fig.4.4. Plane Streaming Kernel vs. Wall Thickness for Duct of Radius r_o = 10 cm

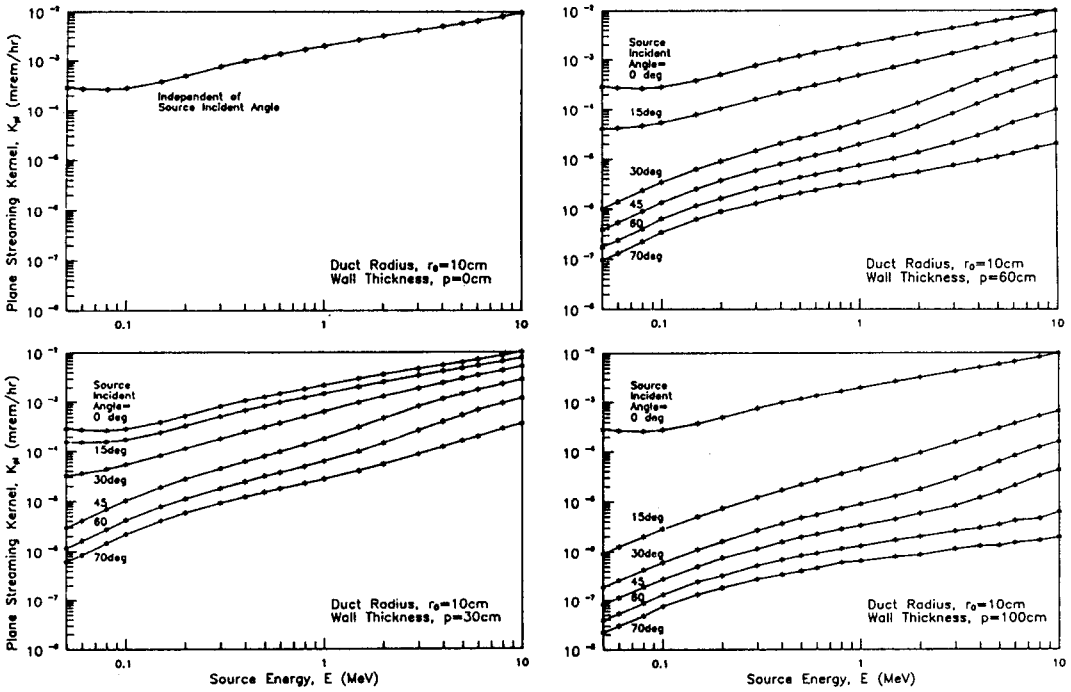

Fig.4.5. Plane Streaming Kernel vs. Source Energy for Duct of Radius $r_o = 10$ cm

wall thickness, source incident angle, and source energy increase, and duct radius decreases. The fact that the relative error R is limited within 5% means that the true solution is within ±5% about the evaluated solution with the confidence of 68%, or within ±10% about the evaluated solution with the confidence of 95%.

5. Approximation of Point Streaming Kernel

The approximation of Eqs. (2.7) and (2.8)—replacement of the material attenuation of a radiant source with one of a parallel source—is accompanied with some error, unless the point source is sufficiently far from the wall. The approximation error in percent, defined as

$$\mathrm{Er} \equiv \frac{K_{pl}(\zeta, E; r_0, p) - K_{pt}(\rho, \zeta, E; r_0, p)}{K_{pt}(\rho, \zeta, E; r_0, p)} \times 100, \quad (5.1)$$

is shown in Table 5.1 for the duct of radius $r_o =$ 20 cm. The error in some cases is too great to justify the approximation. The error occurs from the fact that the incident angle of a particle from a point source varies from place to place where the particle arrives on the wall, while that of a plane source particle invariant. The incident angle of plane source should be carefully selected for the good approximation of point streaming kernel, that might take a value different from the angle ζ of the point source as shown in Figure 2.1. Note that the incident angle of plane source is assumed to be ζ of the point source in Eq. (5.1). If the optimized angle of the plane source is denoted as $\hat{\zeta}$, the exact expression of the approximation becomes, instead of Eqs. (2.7) and (2.8),

$$K_{pt}(\rho, \zeta, E; r_0, p) \approx K_{pl}(\hat{\zeta}, E; r_0, p) \quad (5.2)$$

and

$$X_{pt}(\rho, \zeta, E; r_0, p) \approx \frac{K_{pl}(\hat{\zeta}, E; r_0, p)}{4\pi\rho^2}. \quad (5.3)$$

Let us classify the point sources according to the position of them as shown in Figure 5.1. A point source in Region 1 can see the whole area of the detector surface without any obstruction. Thus let $\hat{\zeta}=0$, since the plane source can see the whole area only when the incident angle is zero. A point source in Region 2 can see only the partial area of the detector surface. It has been demonstrated through several trials that $\hat{\zeta}$ slightly less than the angle ζ_e such that $\rho'_{ct}=1$ mfp, as shown in Figure 5.2, provides a good approximation. A point source in Region 3 cannot see the detector at all. If $\rho'_{ct}\leq 5$mfp, $\hat{\zeta}$ is selected to be slightly less than the angle ζ_t such that $\rho'_{ct}=\rho_{ct}+1$mfp, as shown in Figure 5.3. Otherwise, $\hat{\zeta}$ is determined such that $\rho'_{ct}=6\text{mfp}+0.3(\rho_{ct}-5\text{mfp})$. Here, mfp is mean free path of source particles in concrete, ρ'_{ct} is traverse length through concrete of the line from the source point to the top of the detector, and ρ'_{ct} is that of the line starting from the source point with the desired angle $\hat{\zeta}$. The error after this optimal choice of $\hat{\zeta}$, defined as

$$\widehat{Er} \equiv \frac{K_{pt}(\hat{\zeta}, E; r_0, p) - K_{pt}(\rho, \zeta, E; r_0, p)}{K_{pt}(\rho, \zeta, E; r_0, p)} \times 100, \quad (5.4)$$

is shown in Table 5.2 for the duct of radius $r_o=20$ cm. It was observed that the larger the radius of the duct is, the smaller the error is. For $r_o \geq 10$ cm and $p \leq 100$ cm, the error is below about 30 %, if d/r_o is greater than 6. When d/r_o is less than 6, the error does not exceed 50 %. By using the library of K_{pt}, therefore, a streaming problem can be solved easily with a short time comparable with point kernel method, but with a error smaller than single scattering or Albedo methods, although it should be noted that the error may reach 50 % when the source is close to the inlet of the penetration.

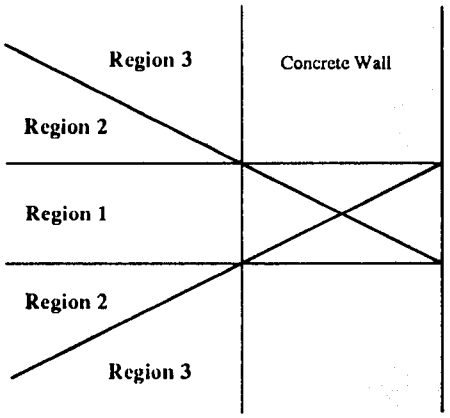

Fig.5.1. Point Source Regions for the Approximation of K_{pt}

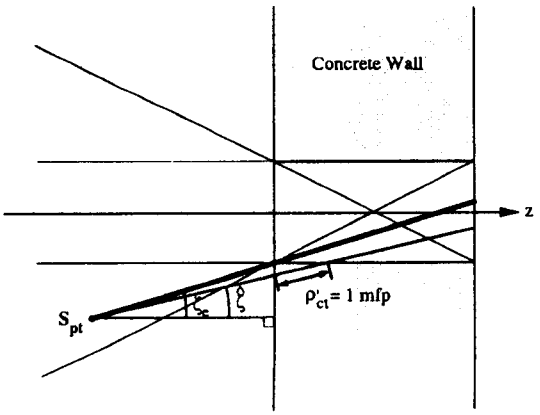

Fig.5.2. When Point Source is in Region 2

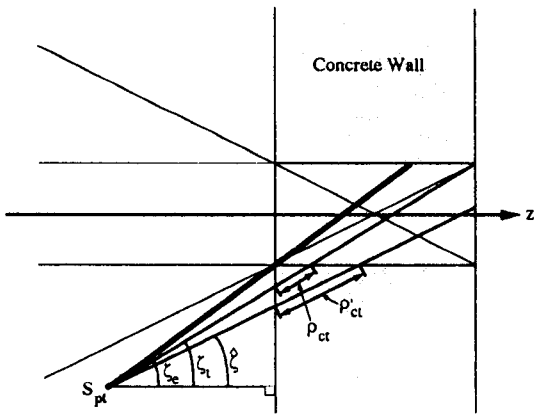

Fig.5.3. When Point Source is in Region 3

Table 5.1. Approximation Error($\widehat{Er}$) for r_0=20 cm Before Optimization

When ζ'=0 degrees and E=1 MeV

d/r_0	p=10 cm	20 cm	30 cm	40 cm	50 cm	60 cm	70 cm	80 cm	90 cm	100 cm
2	11.0	3.5	−4.0	−9.7	−14.1	−16.8	−18.6	−20.3	−21.1	−21.9
4	4.0	−0.1	−4.2	−8.5	−11.0	−13.4	−14.8	−15.5	−16.1	−16.7
6	1.6	−1.3	−4.8	−7.7	−9.8	−11.7	−12.9	−13.6	−14.1	−14.4
8	1.2	−1.1	−3.9	−6.3	−8.2	−9.6	−10.7	−11.1	−11.8	−12.5
10	0.6	−1.3	−3.4	−5.5	−6.7	−7.9	−8.8	−9.7	−9.8	−10.2
12	0.6	−1.1	−3.3	−4.8	−5.8	−7.0	−8.1	−8.2	−8.8	−8.8
14	0.1	−1.3	−2.9	−4.8	−5.6	−6.5	−7.1	−7.4	−8.0	−8.2
16	0.2	−1.2	−2.8	−4.3	−4.8	−5.9	−6.8	−7.0	−6.7	−7.6
18	−0.2	−1.0	−2.1	−3.3	−4.4	−5.4	−6.0	−6.2	−6.5	−7.0
20	0.2	−1.3	−2.1	−3.3	−4.1	−4.9	−5.4	−5.6	−5.8	−6.1
22	0.0	−1.1	−2.2	−3.0	−4.0	−4.6	−5.2	−5.3	−5.6	−5.7
24	−0.1	−0.9	−1.9	−2.8	−3.7	−4.4	−4.8	−5.1	−5.3	−5.8
26	0.1	−1.8	−1.6	−2.7	−3.3	−4.0	−4.5	−4.6	−4.9	−5.0
28	0.0	−0.8	−1.8	−2.6	−3.1	−3.8	−4.0	−4.3	−4.4	−4.9
30	0.0	−0.8	−1.6	−2.4	−2.8	−3.5	−3.8	−4.0	−4.0	−4.5

When ζ'=30 degrees and E=1 MeV

2	2.4	−10.2	−20.6	−28.8	−34.9	−39.0	−42.6	−45.5	−47.8	−49.3
4	−2.2	−8.5	−13.6	−18.4	−21.0	−21.8	−21.2	−18.3	−12.5	−4.9
6	−0.8	−5.9	−10.5	−12.4	−12.4	−10.5	−4.5	5.9	−24.8	56.6
8	−1.3	−5.0	−8.1	−9.2	−7.6	−2.8	6.0	23.6	53.5	88.4
10	−1.2	−4.1	−6.1	−6.5	−4.7	0.2	12.5	33.3	64.2	72.6
12	−1.0	−3.6	−5.7	−5.7	−3.3	2.3	14.3	38.9	60.8	56.0
14	−0.6	−3.0	−4.1	−4.0	−1.6	4.0	16.3	42.3	52.5	36.2
16	−0.4	−2.2	−3.9	−3.0	−0.5	5.7	18.7	41.4	40.7	30.4
18	−1.1	−2.6	−3.5	−2.9	−0.2	6.1	19.4	40.3	28.7	22.1
20	−0.7	−2.0	−3.1	−2.3	0.0	5.1	17.1	35.3	25.7	16.1
22	−0.5	−2.1	−3.2	−2.4	−0.3	4.8	16.4	30.9	21.6	14.5
24	−0.6	−1.8	−2.5	−1.8	0.4	5.7	17.2	27.9	20.0	15.1
26	−0.7	−1.9	−2.4	−1.8	0.8	5.8	17.0	24.0	15.2	12.7
28	=0.3	−1.5	−2.5	−1.2	0.7	6.8	18.0	24.2	13.0	12.4
30	−0.7	−1.3	−2.2	−1.7	0.7	5.2	16.2	21.3	10.2	8.8

When ζ'=60 degrees and E=1 MeV

2	−10.4	−15.5	−14.0	−6.9	11.4	38.4	67.3	98.5	132.5	165.3
4	−6.6	−1.3	24.7	63.1	67.7	65.0	62.9	66.6	75.0	81.3
6	−3.7	4.7	39.9	39.3	38.3	44.2	53.5	64.5	74.4	81.0
8	−3.1	5.2	34.5	26.7	30.3	39.5	47.6	54.8	62.7	72.0
10	−2.3	5.9	27.7	22.4	26.9	34.7	43.1	50.5	59.1	65.8
12	−1.8	6.8	21.3	19.0	2.9	32.2	39.0	46.0	54.0	63.2
14	−1.3	6.0	19.0	17.2	23.4	31.2	38.1	43.5	50.2	58.8
16	−1.4	5.2	15.0	14.5	20.0	27.2	32.4	38.6	43.2	48.7
18	−1.1	5.9	13.3	15.4	21.3	27.7	32.3	37.6	42.8	48.4
20	−1.2	4.0	11.6	11.8	17.1	22.5	26.1	31.4	35.0	39.2
22	−2.2	4.2	10.5	11.6	16.4	22.6	27.3	30.8	36.4	40.3
24	−1.3	4.0	10.7	11.4	16.3	20.9	26.5	29.9	35.3	37.4
26	−0.8	4.1	8.5	9.3	14.1	17.6	23.0	26.8	31.8	35.8
28	−0.7	3.5	7.1	8.1	11.2	16.4	20.5	25.0	29.4	32.3
30	−0.1	3.6	7.0	8.1	11.4	15.6	20.0	23.3	26.0	29.4

Table 5.2. Approximation Error($\hat{Er}$) for r_o=20 cm Before Optimization

When ζ'=0 degrees and E=1 MeV

d/r_m	p=10 cm	20 cm	30 cm	40 cm	50 cm	60 cm	70 cm	80 cm	90 cm	100 cm
2	11.0	3.5	−4.0	−9.7	−14.1	−16.8	−18.6	−20.3	−21.1	−21.9
4	4.0	−0.1	−4.2	−8.5	−11.0	−13.4	−14.8	−15.5	−16.1	−16.7
6	1.6	−1.3	−4.8	−7.7	−9.8	−11.7	−12.9	−13.6	−14.1	−14.4
8	1.2	−1.1	−3.9	−6.3	−8.2	−9.6	−10.7	−11.1	−11.8	−12.5
10	0.6	−1.3	−3.4	−5.5	−6.7	−7.9	−8.8	−9.7	−9.9	−10.2
12	0.6	−1.1	−3.3	−4.8	−5.8	−7.0	−8.1	−8.2	−8.8	−8.8
14	0.1	−1.3	−2.9	−4.8	−5.6	−6.5	−7.1	−7.4	−8.0	−8.2
16	0.2	−1.2	−2.8	−4.3	−4.8	−5.9	−6.8	−7.0	−6.7	−7.6
18	−0.2	−1.0	−2.1	−3.3	−4.4	−5.4	−6.0	−6.2	−6.5	−7.0
20	0.2	−1.3	−2.1	−3.2	−4.1	−4.9	−5.4	−5.6	−5.8	−6.1
22	0.0	−1.1	−2.2	−3.0	−4.0	−4.6	−5.2	−5.3	−5.6	−5.7
24	−0.1	−0.9	−1.9	−2.8	−3.7	−4.4	−4.8	−5.1	−5.3	−5.8
0.1	−0.8	−1.6	−2.7	−3.3	−4.0	−4.5	−4.6	−4.6	−5.0	
28	0.0	−0.8	−1.8	−2.6	−3.1	−3.8	−4.0	−4.3	−4.4	−4.9
0.0	−0.8	−1.6	−2.4	−2.4	−3.5	−3.8	−4.0	−4.0	−4.5	

When ζ'=30 degrees and E=1 MeV

2	7.9	2.9	−2.3	−7.1	−10.7	−12.8	−14.8	−15.8	−17.0	−17.4
4	2.2	−0.1	−3.0	−6.0	−9.5	−12.3	−14.6	−17.0	−18.5	−21.0
6	1.5	−0.3	−2.6	−5.0	−7.1	−9.7	=12.1	−14.6	−18.9	−25.2
8	0.6	−0.4	−1.9	−4.0	−5.4	−6.8	−9.0	−12.4	−18.8	−21.3
10	0.5	−0.7	−1.9	−3.2	−4.3	−6.5	−8.4	−12.5	−18.8	−15.7
12	0.4	−0.4	−2.2	−3.3	−3.8	−5.5	−8.2	−12.0	−14.2	−15.2
14	0.5	0.0	−0.9	−1.9	−2.7	−4.6	−7.3	−12.2	−11.1	−12.0
16	0.6	0.5	−1.1	−1.2	−2.1	−3.3	−5.6	−10.7	−9.9	−9.3
18	−0.2	−0.4	−1.0	−1.4	−2.0	−2.8	−4.6	−7.6	−10.5	−8.5
20	0.1	0.0	−0.9	−0.9	−1.1	−1.8	−3.7	−5.8	−7.1	−8.8
22	0.3	−0.4	−1.2	−1.4	−2.2	−3.7	−5.7	−6.4	−8.1	−7.6
24	0.2	−0.2	−0.7	−0.9	−1.5	−2.8	−4.7	−4.9	−5.6	−5.1
26	0.0	−0.5	−0.7	−1.1	−1.2	−2.5	−4.6	−5.4	−6.0	−5.1
28	0.4	−0.2	−1.0	−0.5	−1.3	−1.4	−3.5	−4.6	−4.4	−3.5
30	0.0	−0.2	−0.7	−1.1	−1.3	−2.6	−4.5	−6.2	−5.9	−4.09

When ζ'=60 degrees and E=1 MeV

2	1.8	2.7	−0.8	−6.7	−14.9	−16.0	−10.5	−6.7	−4.5	−4.5
4	2.1	3.2	−5.7	−10.0	−10.4	−5.7	0.7	7.3	3.2	−2.4
6	2.4	2.9	−5.6	−4.8	1.7	10.1	12.2	10.5	−7.3	3.0
8	1.3	1.2	−5.7	−2.0	6.1	11.1	9.5	6.1	5.0	4.4
10	1.3	1.2	−3.6	1.4	9.4	10.0	8.6	7.3	4.8	3.4
12	1.2	1.5	−3.7	2.1	9.6	9.9	8.5	8.1	6.5	5.0
14	1.1	0.9	−2.4	3.4	9.3	10.4	10.4	9.3	8.8	8.2
16	0.6	0.2	−2.3	3.0	6.9	7.8	8.3	8.1	7.9	6.5
18	0.5	1.1	−0.9	4.6	9.0	9.6	9.8	9.3	10.2	10.9
20	0.2	−0.5	−1.6	2.4	5.9	6.3	5.9	6.1	6.2	6.5
22	0.1	−0.1	−1.9	3.4	5.6	7.4	7.5	7.1	7.8	9.6
24	−0.2	−0.1	−1.0	4.1	6.4	6.7	7.3	7.0	7.5	7.6
26	0.3	0.3	−2.4	2.6	5.1	4.5	4.8	4.9	5.1	6.7
28	0.3	−0.1	−2.5	1.8	3.1	4.1	3.7	3.9	3.5	4.3
30	0.8	0.1	−1.5	2.1	3.9	4.1	4.3	3.5	1.5	2.4

6. Conclusions

For radiation streaming problems through a straight cylindrical duct within concrete walls due to a broad, monodirectional, monoenergetic gamma-ray plane source, a Monte Carlo method was developed as described in Section 3. A data library of plane streaming kernel, which is evaluated by the Monte Carlo method, was constructed as summarized in Section 4. The data library can be used to approximate point streaming kernel for a point isotropic gamma-ray source located at arbitrary place inside the wall with a reasonnable error as described in Section 5.

The library can be used for the efficient and accurate analysis of streaming problems having gamma-ray source of arbitrary distribution whose infinitesimal volume is thought to be an isotropic point source. The total contribution from the source distribution is then obtained by a simple integration of

$$\begin{aligned} X &= \int_{V_s}\int_{E_s} X_{pt}(\rho,\varsigma,E;r_0,p)S(\rho,\varsigma,E)\,dV_s(\rho,\varsigma)\,dE \\ &= \int_{V_s}\int_{E_s} \frac{K_{pt}(\rho,\varsigma,E;r_0,p)}{4\pi\rho^2}S(\rho,\varsigma,E)\,dV_s(\rho,\varsigma)\,dE \\ &\approx \int_{V_s}\int_{E_s} \frac{K_{pl}(\hat{\varsigma},E;r_0,p)}{4\pi\rho^2}S(\rho,\varsigma,E)\,dV_s(\rho,\varsigma)\,dE \end{aligned} \tag{6.1}$$

where X is the average dose rate over the duct crosssectional area at duct outlet, and $S(\rho, \zeta, E)$ is the source distribution over the volume V_s and in the energy range E_s, and K_{pl} is the data library of plane streaming kernels obtained in this study.

References

1. R. E. Malenfant, "G^3 : A General Purpose Gamma-Ray Scattering Program," LA-5176, Los Alamos Scientific Laboratory (1973)
2. N. M. Schaeffer, *Reactor Shielding for Nuclear Engineers,* TID-25951 (1973)
3. J. M. Chapman and C. M. Huddleston, "Dose Attenuation in Two-Legged Concrete Ducts for Various Gamma-Ray Energies," *Nucl. Sci. Eng.*, **25**, 66 (1966)
4. L. L. Carter and E. D. Cashwell, *Particle Transport Simulation with the Monte Carlo Method,* TID-26607 (1975)
5. E. D. Cashwell and C. J. Everett, *A Practical Manual on the Monte Carlo Method for Random Walk Problems,* Pergamon Press Inc. (1959)
6. J. F. Briesmeister, Editor, "MCNP–A General Monte Carlo Code for Neutron and Photon Transport," LA-7396-M, Version 3A, Los Alamos National Laboratory (1986)
7. E. A. Straker, P. N. Stevens, D. C. Irving, and V. R. Cain, "MORSE-CG–General Purpose Monte Carlo Multigroup Neutron and Gamma-Ray Transport Code," CCC-203, Oak Ridge National Laboratory, Radiation Shielding Information Center (1973)
8. J. Spanier and E. M. Gelbard, *Monte Carlo Principles and Neutron Transport Problems,* Addison-Wesley Publishing Co. (1969)
9. J. Wood, *Computational Methods in Reactor Shielding,* Pergamon Press Inc. (1982)
10. ANS Working Group 6.4.1, "Guidelines on the Nuclear Analysis and Design of Concrete Radiation Shielding for Nuclear Power Plants," ANSI/ANS-6.4-1985, American Nuclear Society (1985)
11. ANS Working Group 6.1.1, "Neutron and Gamma-Ray Flux-to-Dose Rate Factors," ANSI/ANS-6.1.1-1977, American Nuclear Society (1977)
12. H. Kahn, "Application of Monte Carlo," AECU-3259, Rand Corporation (1954)
13. R. N. Blomquist and E. M. Gelbard, "An Assessment of Existing Klein-Nishina Monte Carlo Sampling Methods," *Nucl. Sci. Eng.*, **83**, 380 (1983)
14. F. H. Clark, "Variance of Certain Flux Estimators Used in Monte Carlo Calculations," *Nucl. Sci. Eng.*, **27**, 235 (1967)